Supporting Information

Cyclic voltammetry electrodeposition of well-dispersed Pd nanoparticles in carbon paper as a flow-through anode for a microfluidic direct formate fuel cell

Tong Zhang,[a,b] Xun Zhu,[*a,b] Ding-Ding Ye,[*a,b] Rong Chen,[a,b] Yuan Zhou,[a,b] Qiang Liao,[a,b]

[a] Key Laboratory of Low-grade Energy Utilization Technologies and Systems (Chongqing University), Ministry of Education, Chongqing 400030, China.

[b] Institute of Engineering Thermophysics, School of Energy and Power Engineering, Chongqing University, Chongqing 400030, China

* Corresponding Authors: Xun Zhu, Dingding Ye

E-mail address: **zhuxun@cqu.edu.cn** (X. Zhu), dingdingye@cqu.edu.cn (D.-D. Ye)

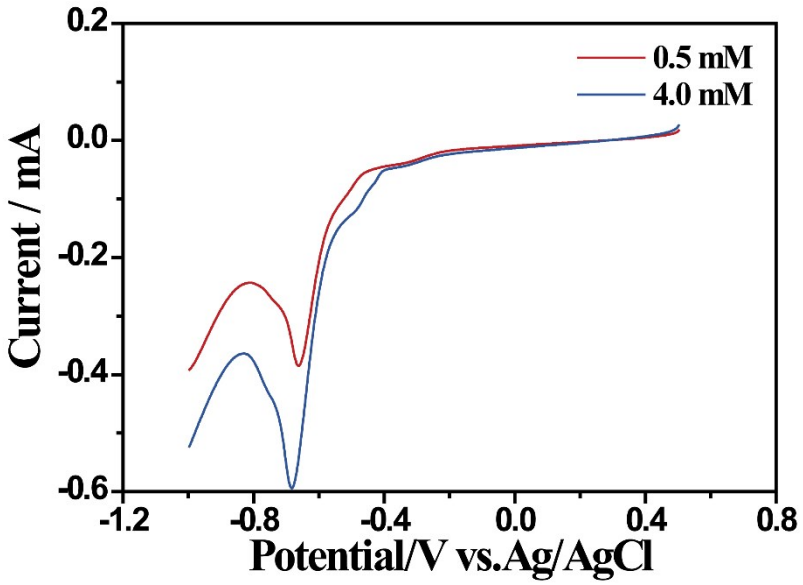

Figure S1 Linear sweep voltammetry curves in different concentrations of Pd^{2+} at a scan rate of 100mV s^{-1}

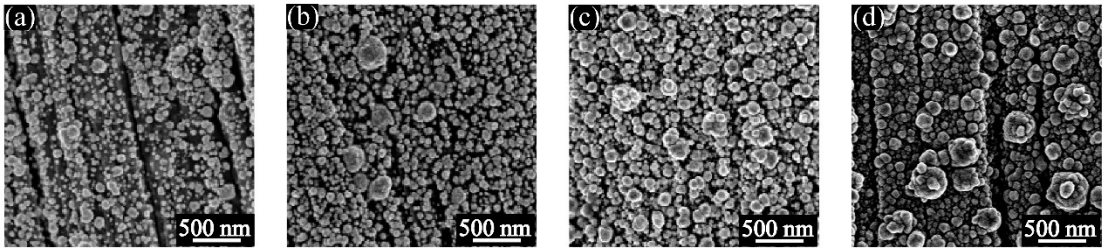

Figure S2 Surface SEM images of the electrodes prepared by electrodeposition in different $Pd(NH_3)_4Cl_2$ concentrations (a) 0.5 mM (b) 1 mM (c) 2 mM (d) 4 mM.

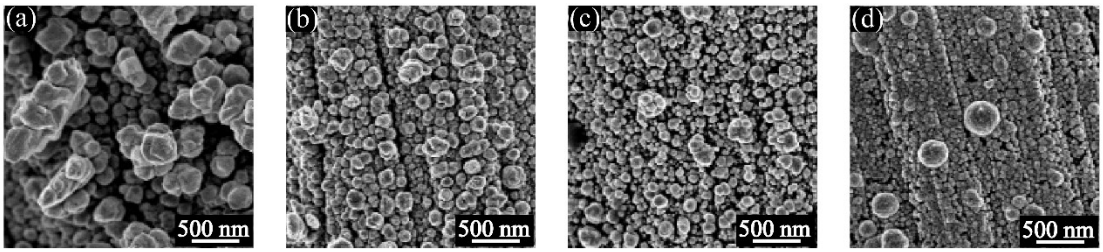

Figure S3 The morphology of Pd catalyst particles on the electrodes prepared by electrodeposition in different scan rates (a) 1.0 mV s^{-1} (b) 2.5 mV s^{-1} (c) 5.0 mV s^{-1} (d) 10 mV s^{-1}.

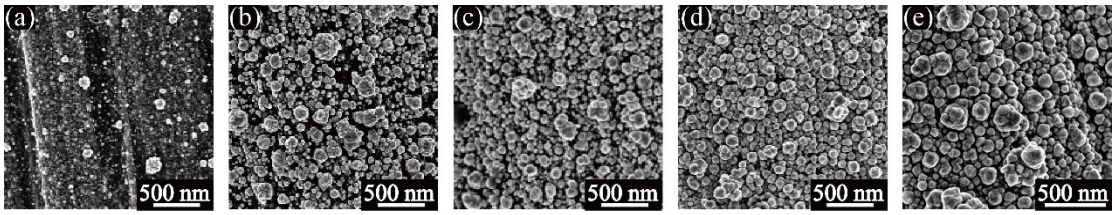

Figure S4 Surface SEM images of the electrodes prepared by electrodeposition with different cycle numbers (a) 1 cycle (b) 3 cycles (c) 5 cycles (d) 7 cycles (e) 10 cycles.

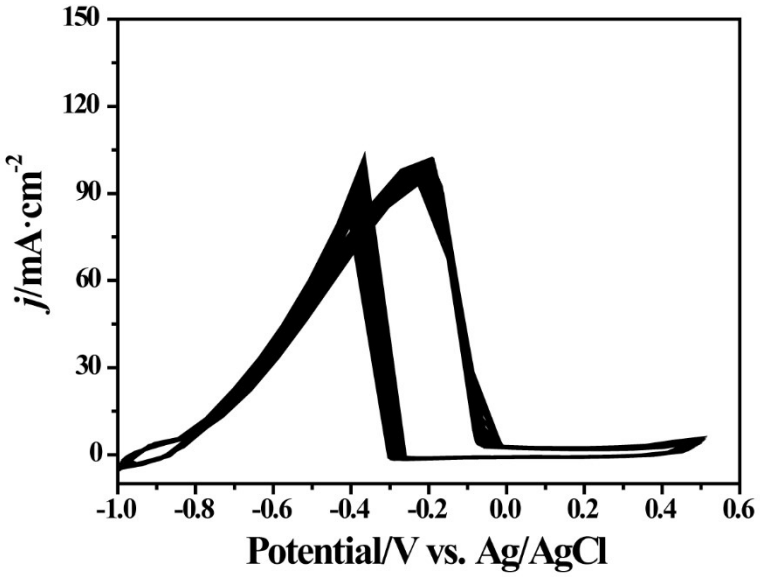

Figure S5 50 cycles in the presence of 1 M KOH + 0.5 M HCOONa at a scan rate of 10 mV s^{-1}.

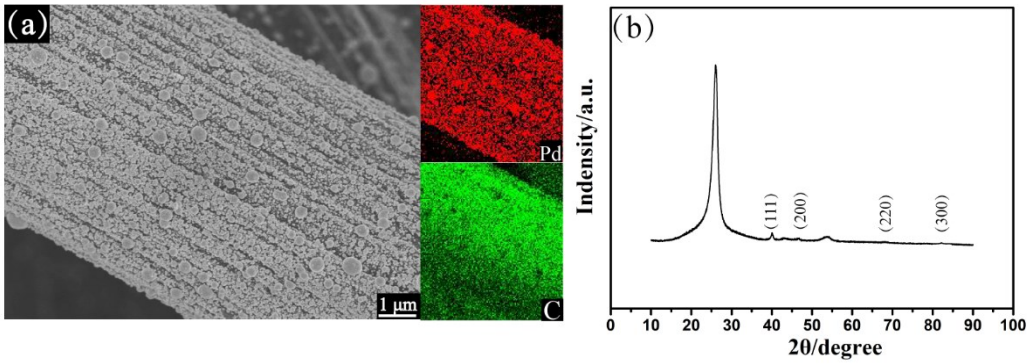

Figure S6 (a) SEM images and (b) XRD patterns of the Pd/CP electrode after CV test. Insets are corresponding EDS elemental mapping.

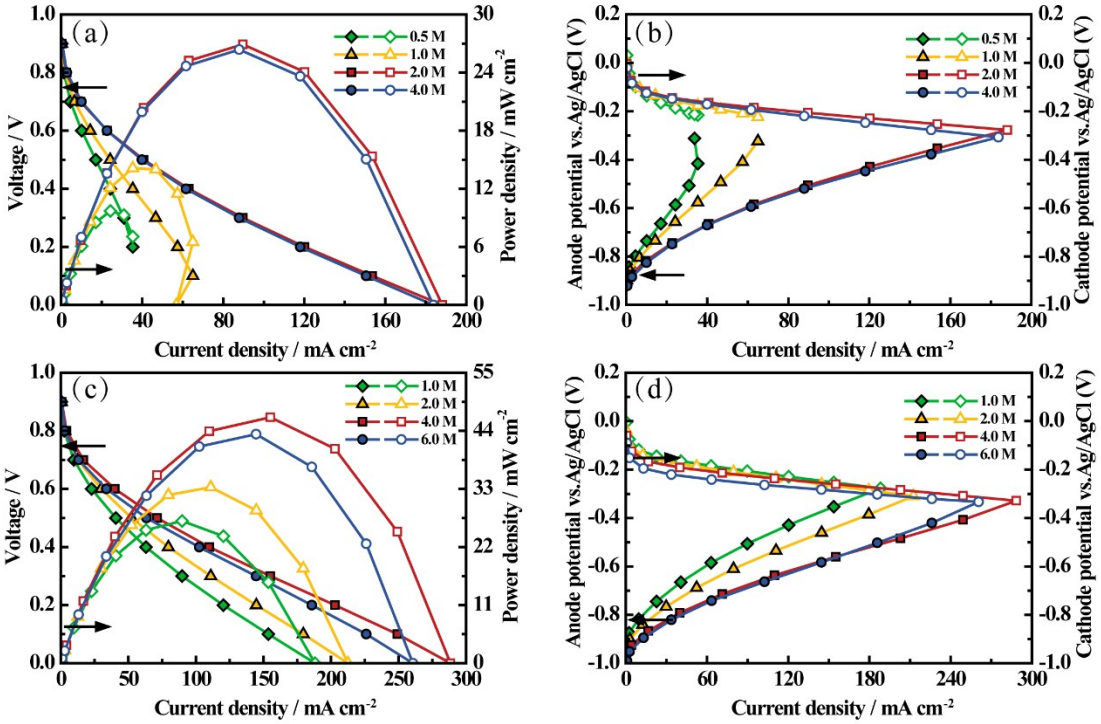

Figure S7(a) Polarization curves and (b) electrode potentials of the μDFFC operating in different fuel concentrations. (c) Polarization curves and (d) electrode potentials of the μDFFC operating in different electrolyte concentrations.

Figure S7 showed the fuel cell performance operating in different fuel and electrolyte concentration. Figure S7a and S7b show the cell performance measured at different fuel concentrations with 1 M KOH served as electrolyte, and the flow rate was kept at 200 μl min^{-1}. From the Figure S7a, the peak power density of the fuel cell increases obviously from 9.72 mW cm^{-2} to 14.1 mW cm^{-2} and 26.9 mW cm^{-2} with increasing the fuel concentration form 0.5 M to 2 M. However, when the fuel concentration was increased to 4 M, the peak power density is 26.3 mW cm^{-2}, and the maximum current density is 183.7 mA cm^{-2}, which is a little lower than that at 2 M. It is note from Figure S7b that the cathode potential declined when the fuel concentration was increased from 2 M to 4 M. This demonstrates that fuel crossover occurred at higher fuel concentration, which reduces the cell

performance. The effect of electrolyte concentration on fuel cell performance was shown in Figure S7c and S7d. The fuel concentration was kept at 2 M and the flow rate was also maintained at 200 μl min^{-1}. The cell performance increases with increase of electrolyte concentration, but is capped at electrolyte concentration over 4 M. The peak power density increases from 26.9 mW cm^{-2} to 33.3 mW cm^{-2} and 46.6 mW cm^{-2} while the maximum current density of the fuel cell climbs from 188.1 mA cm^{-2} to 212.6 mA cm^{-2} and 288.4 mA cm^{-2} when electrolyte concentration increases from 1 M to 3 M. The improvement of cell can be attributed to the increased ionic conductivity of the electrolyte with more hydroxyl ions and the enhanced anode reaction kinetics in higher concentration of KOH. Nevertheless, the cell performance reduces when the electrolyte increases to 6 M. The peak power density and maximum current density drop to 43.3 mW cm^{-2} and 260.6 mA cm^{-2}, respectively. As shown in Figure S7d, when the electrolyte concentration changes from 4 M to 6 M, the cathode potential declines. The weakened cell performance is due to higher hydroxide ion concentration can suppress the cathode reaction kinetic [1].

Table S1 Comparison of the cell performance of this work with other microfluidic fuel cells reported in the literatures

References	Electrolyte	Oxidant	Fuel	Catalyst loading (anode) (mg_{Pd} cm^{-2})	Imax (mA cm-2)	P_{max} (mW cm^{-2})
Kjeang et al. [2]	NaOH	NaClO	HCOONa	5	230	52
Nguyen et al. [3]	H_2SO_4	Air	HCOOH	7-8	120	26.5
Chavez-Ramírez et al. [4]	H_2SO_4	Air	HCOOH	1	152	27.3
Sung et al. [5]	H_2SO_4	$KMnO_4$	HCOOH	No date	37	13

Alonso-Vante et al. [6]	H_2SO_4	O_2	HCOOH	5	102	23
Ye et al. [7]	NaOH	H_2O_2	HCOONa	5	56.6	20.7
This work	**NaOH**	**Air**	**HCOONa**	**0.105**	**288.4**	**46.6**

Supplementary References

1. B. Zhang, D.-D. Ye, J. Li, X. Zhu and Q. Liao, *Electrochimical Acta*, 2015, **177**, 264-269.
2. E. Kjeang, R. Michel, D. A. Harrington, D. Sinton and N. Djilali, *Electrochimical Acta*, 2008, **54**, 698-705.
3. S. A. M. Shaegh, N.-T. Nguyen, S. H. Chan and W. Zhou, *International journal of hydrogen energy*, 2012, **37**, 3466-3476.
4. A. Moreno-Zuria, A. Dector, F. Cuevas-Muñiz, J. Esquivel, N. Sabaté, J. Ledesma-García, L. Arriaga and A. Chávez-Ramírez, *Journal of power sources*, 2014, **269**, 783-788.
5. H. B. Park, K. H. Lee and H. J. Sung, *Journal of power sources*, 2013, **226**, 266-271.
6. J. Ma, A. S. Gago and N. Alonso-Vante, *Journal of The Electrochemical Society*, 2013, **160**, F859-F866.
7. Z. Liu, D. Ye, R. Chen, B. Zhang, X. Zhu, J. Li and Q. Liao, *International Journal of Hydrogen Energy*, 2018, **43**, 22467-22473.